Mechanics of Materials 184 (2023) 104746

Contents lists available at ScienceDirect

Mechanics of Materials

journal homepage: www.elsevier.com/locate/mechmat

Research paper

Which asperity scales matter for true contact area? A multi-scale and statistical investigation

R.L. Jackson [a,*], T.D.B. Jacobs [b]

[a] Department of Mechanical Engineering, Auburn University, Auburn, AL, 36849, USA
[b] Department of Mechanical Engineering and Material Science, University of Pittsburgh, Pittsburgh, PA, 15261, USA

ARTICLE INFO

Keywords:
Contact
Contact mechanics
Rough surfaces
Roughness

ABSTRACT

The true contact area between two surfaces is only a small fraction of the apparent macroscopic contact area; it governs many interfacial properties such as friction and contact resistance and depends sensitively on roughness. However, for real-world multi-scale surface topography, it is not clear which size scales of roughness govern the true contact area. This study investigates true contact area for a real-world surface that has been characterized across all scales from Angstroms to centimeters. Elastic and elastic-plastic contact is investigated using both a multiscale framework and a statistical roughness model. The multiscale method is a rough-surface contact-modeling technique based on Archard's stacked scales from a spectrum of the surfaces, which has shown promise when compared to previous experimental and numerical results. In contrast, statistical models assume that the asperities follow a defined height distribution and are in contact when taller than the mean surface separation. The results show that even the smallest scales can have a significant influence on the contact area, especially when the contact is elastic. However, when the contact is elastic-plastic, the influence of smaller scales can be limited depending on the character of the roughness. For self-similar, fractal-like roughness across some scales, the pressure tends to saturate at those scales. This work also explores the inclusion of scale-dependent yield strength. Both the multiscale and statistical models predict that the inclusion of scale-dependent strength causes the predicted contact area of the elastic-plastic models to come into closer agreement with that of the elastic model, especially when a wider range of size scales are included. In addition, both types of models predict that below a certain scale, smaller asperities flatten under contact pressure and will no longer influence the predicted contact area. Taken together, this work helps to guide the accurate modeling of rough-surface contact, and provides insights into which scales can be modified to improve performance in manufactured components.

1. Introduction

Surface topography governs the performance of rough contacts. This has been clear since Coulomb suggested that roughness and the real area of contact played a role in the magnitude of friction between solids and, later, when Tabor and Bowden provided an in-depth analysis of the role roughness plays in the mechanism of friction (Bowden and Tabor, 1939). The importance of roughness in predicting friction has continued to more recent models of static friction (Patil and Eriten, 2014). It is straightforward to predict the dependence of contact properties on simple models of roughness, such as single-scale sinusoids. However, the prediction of roughness-dependent surface properties is complicated by the fact that real-world surface roughness exists across many different length scales. Recently, several approaches have been developed to account for multi-scale roughness; with a useful comparison published recently to show how different models agree and differ (Müser et al., 2017; Müser and Nicola, 2022). There have been several fractal-based multiscale models of rough-surface contact, such as where Majumdar and Bhushan (1991) used truncation of the fractal with a flat to predict contact area. Persson (2006) also developed a popular multiscale contact model that uses a diffusion theory to solve the elastic contact of self-affine fractal-like surfaces. Another type of multiscale model evolved from Archard's (Archard, 1957) stacked-asperity model that assumes all asperities of a certain size are stacked on top of larger asperities. Therefore, each scale of asperities carries the same load (i.e., different scales are in mechanical series). That load is then distributed uniformly over all of the asperities on each scale (i.e., individual asperities are in mechanical parallel). Ciavarella and Demelio (2001)

* Corresponding author.
E-mail address: jackson@auburn.edu (R.L. Jackson).

https://doi.org/10.1016/j.mechmat.2023.104746
Received 28 February 2023; Received in revised form 30 May 2023; Accepted 10 July 2023
Available online 14 July 2023

developed this further for fractal elastic contact and later Jackson and Streator (2006) extended the concept to measured surface spectra and elasto-plastic asperities. In simplifying this stacked multiscale contact method it was proposed that the key parameter of describing rough-surface contact is the upper limit of roughness within the flattening contact areas (Jackson, 2010a; Jackson et al., 2009). These are the tallest and most acute peaks that require the highest pressure to be compressed within the contact areas. While the statistical and multiscale models discussed above differ from the versions used in Muser et al. (Müser et al., 2017), one of the stacked multiscale models used in that work agreed closely with the predictions of Green's function molecular dynamics. However, a key remaining question is which size scales must be considered and included to accurately predict the roughness-dependent contact area.

One limitation of some of the prior work on roughness-dependent properties is its reliance on the assumption of self-affine fractal-like roughness. While experimental measurements of the real contact area at the nanoscale show what appears to be a fractal-like structure (Xu et al., 2018, 2020) (similar to the islands and coastlines originally used by Mandelbrot (1967) to conceptualize fractals and by Richardson who observed the phenomenon (Richardson, 1961)), there remain questions about the fidelity of fractals to real surfaces. Notably, natural surfaces may have multi-scale roughness but still not adhere to fractal-like self-affinity (Borodich et al., 2016; Whitehouse, 2001; Zhang and Jackson, 2017), or may be difficult to effectively characterize experimentally due to instrument limitations (Jacobs et al., 2017). It is well known that the conventional surface parameters such as roughness, slope and curvature all change with scale. In contrast, the idea of characterizing a surface as a fractal is powerful if it can provide a scale-independent parameter. Whitehouse argued that fractals are not particularly useful unless this is true (Whitehouse, 2001). He also showed that typical engineering surfaces follow a Markov process and produce at least surfaces with a bi-fractal spectrum, if not more variations with scale. This same multi-fractal structure has been observed by others as well on both manufactured and natural surfaces (Borri and Paggi, 2015; Bhushan and Majumdar, 1992).

Another limitation of much of the prior work is the assumption of a single value of strength, regardless of size-scale. Since the features or asperities of rough surfaces are composed of a wide range of scales, the scale-dependence of material properties becomes important. The "smaller-is-stronger" trend is well established in the nanomechanics community and is often attributed to a starvation of dislocations and sources in small volumes. The effective yield strength, especially, will most likely increase with smaller scales (Broitman, 2016). The limitations of indentation measurements due to scale effects were reviewed by Broitman (2016). Concepts such as dislocation-based and strain-gradient theories can be used to account for these scale-dependent strengths in continuum contact models of rough surfaces (Jackson, 2006). For instance, strain-gradient plasticity was employed in a recent investigation using a fractal contact model to incorporate the scale-dependent strength (Zhang et al., 2022). That investigation showed that the inclusion of strain-gradient plasticity resulted in a four-fold increase in the asperity contact pressure past the conventional hardness.

In another example showing scale-dependent strength, Venugopalan and Nicola (2019) used Green's function dislocation dynamics to describe an indenter with self-affine roughness. Surprisingly, due to limited dislocation availability and geometric effects, Venugopalan and Nicola predicted contact pressures up to 40 times larger than conventional hardness. Geometric effects such as fractal-driven sharp asperity aspect ratios and asperity coalescence can increase the contact pressure in addition to scale-dependent plasticity. These results confirm the predictions of previous continuum asperity and rough-surface contact models (Jackson, 2006; Jackson et al., 2015; Krithivasan and Jackson, 2007; Manners, 2008). These investigations find that the hardness or material strength in fractal models of rough-surface contact must be adjusted for scale and shape effects (Venugopalan et al., 2019). Therefore, one of the aims of the current work is to include scale-dependent plasticity in rough-surface contact analysis while considering a wider range of roughness scales.

Although adhesion is not included in the current work, previous investigations have examined the influence of scales of roughness on elastic adhesive contact (Papangelo and Ciavarella, 2021; Violano et al., 2021). They found that for soft surfaces that the adhesion persists with little influence of the range of roughness included in the analysis (Violano et al., 2021). In the more recent work (Papangelo and Ciavarella, 2021), the same nearly complete surface spectrum considered in the current work is employed. Through comparison to experimental results (Dalvi et al., 2019), they also found that several models adequately predicted the adhesion between the surfaces for the case of loading (Persson and Tosatti, 2001). However, for unloading the results are not as straightforward due to hysteresis. Regardless, they provide fitting models that predict the experimentally measured adhesion down to extremely small scales.

The purpose of the present investigation is to elucidate the contribution to elastic-plastic real contact area by different size scales of roughness. This will be achieved by using two different modeling approaches, a stacked multiscale model and a statistical model, and by addressing the two aforementioned limitations of some of the prior work: the assumption of fractal-like roughness and the assumption of scale-invariant strength. To eliminate the fractal-like assumption, we will use a comprehensive characterization of a real-world surface by Gujrati et al. (2018) that combined transmission electron microscopy with conventional techniques to characterize roughness spanning eight orders of magnitude in size. The authors published their work using the freely available web application contact.engineering (Röttger et al., 2022) and thus, all data and the measurements and characterization tools from that investigation are publicly available (Gujrati et al., 2022a). The statistical models will consider both spherical and sinusoidal asperities. The present analysis was also run with and without an accounting for scale-dependent strength.

2. Analysis of surface-topography data

This work uses as raw input the composite power spectral density *PSD* from Gujrati et al. (2018) in its analysis of surface parameters and rough-surface contact. The power spectral density is a mathematical tool that separates contributions from different length scales, and is equal to the square of the Fourier transform of the measured surface heights (Jacobs et al., 2017). It can be computed for individual measurements, but also presents a useful method for combining many measurements

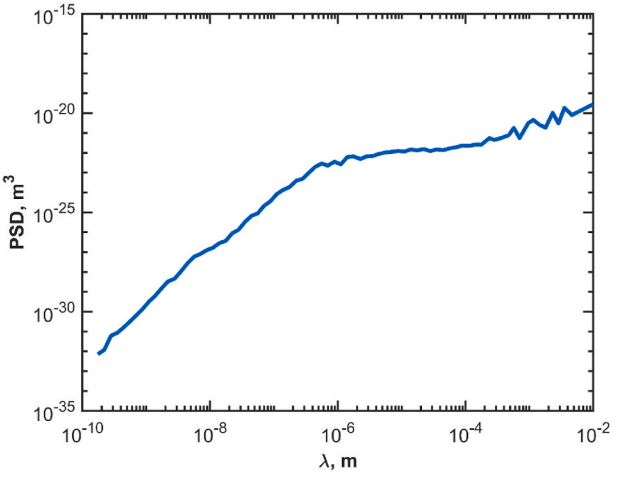

Fig. 1. The composite power spectrum of a surface obtained by multiple measurements from different instruments.

across different scales. The composite spectrum, shown in Fig. 1, is the log-space average of all individual measurements from stylus profilometry, atomic force microscopy, and transmission electron microscopy. All raw data associated with the original surface can be accessed at Ref. [37].

In several previous studies (Kogut and Jackson, 2005; Sayles and Thomas, 1978), it has been shown that many surface roughness and statistical parameters vary with scale. This was one of the driving factors giving rise to the usage of fractals for describing surfaces (Majumdar and Tien, 1990). In the paper by Kogut and Jackson (2005), the trends of the spectral moments were only examined over two orders of magnitude of length scale from a generated fractal surface. The statistical variance m_0 changed least with the inclusion of smaller scales, but m_2 and m_4 both changed by many orders of magnitude. Later, Green provided closed-form solutions to the spectral moments of fractal surfaces following the Weierstrass-Mandelbrot formulation (Green, 2019). Brown et al. reviewed the methods to characterize multiscale surfaces (Christopher et al., 2018). According to Parseval's law, surface descriptors should be able to be calculated equivalently in real- or frequency-space, although Kalin et al. (2016) showed that the spectral-based parameters of rough surfaces often differ from those acquired directly from the surface by deterministic counting of the asperities. They attribute the differences to varying definitions of asperity-peaks between deterministic and statistical analysis.

For the present modeling approach, scale-dependent moments were calculated, and then used to compute key roughness descriptors using the method of McCool (1986). First, spectral moments from the composite spectrum were computed according to Gujrati et al. (2018):

$$m_k = \int_{\lambda_c}^{\lambda_u} (2\pi)^{k+1} (\lambda)^{-(2+k)} PSD \cdot d\lambda \tag{1}$$

The wavevector ω is often used in previous literature (Gujrati et al., 2018) and is related to the wavelength λ by $\omega = 2\pi/\lambda$. Equation (1) is numerically integrated to obtain the needed spectral moments (m_0, m_2 and m_4) over the range of scales available, i.e. between λ_u and λ_c, the upper and lower limit of the wavelengths of the composite spectrum. Ideally, λ_u is ∞ and λ_c is 0, but this is not obtainable for experimental surface data. λ_c is also referred to as the cut-off wavelength and represents the smallest scale of roughness considered.

The results of this integration agree well with the real-space surface parameters measured directly in Gujrati et al. (2018). By interrupting the integration given in Eq. (1) at different ranges of scale, or in other words by varying λ_c, one can evaluate the influence of smaller and smaller surface features as compared to what was available in prior studies that used conventional topography measurements. The results of this analysis are shown in Fig. 2. These scale-dependent spectral moments are similar to the scale-dependent roughness parameters discussed in Sanner et al. (2022) and for other surfaces in a previous work (Kogut and Jackson, 2005). The results show that the moments can change by many orders of magnitude with the inclusion of increasing details of roughness (especially m_2 and m_4).

The aforementioned spectral moments are related to real-space parameters to be used as inputs to the statistical model using the approach of McCool (1982). In the current work, the statistical model will consider both spherical and sinusoidal shaped asperities, and therefore we will start with the original parameters of the spherical asperity-based statistical models. The expression of m_0 is the same as the square of the RMS roughness, R_q, i.e., $m_0 = (R_q)^2$ (Patil and Eriten, 2014). The moment m_2 is related to the RMS slope, $\bar{g}$, of a line contour such that (note that for a surface a factor of $\sqrt{2}$ must be included)

$$\bar{g} = \sqrt{m_2} \tag{2}$$

Finally, the moment m_4 is related to the RMS curvature of the surface. However, to find the RMS radius of curvature at the tips of the asperities on the surface, the following equation from McCool (1987) is employed. This will be used later when employing the statistical contact model to evaluate the effect of roughness on contact area.

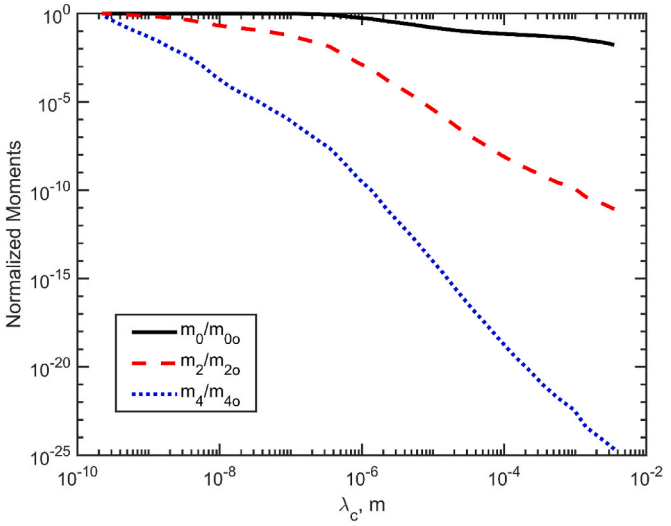

Fig. 2. The normalized spectral moment obtained from the composite spectrum as increasingly smaller scales of roughness are included (indicated by wavelength).

$$R = 0.375\sqrt{\frac{\pi}{m_4}} \tag{3}$$

in addition, the areal asperity density is computed as:

$$\eta = \frac{m_4}{6\pi\sqrt{3}m_2} \tag{4}$$

The elastic modulus, E, and the Poisson's ratio, ν, of the UNCD material is taken to be 463 GPa and 0.20, respectively, from Ref. (Mohr et al., 2014). Following the same work, the strength of the UNCD is 1.8 GPa. The composite modulus E^* between the surfaces is then calculated by assuming that the opposing surface is rigid.

Another method to evaluate the surfaces is to compute the *amplitude spectrum* of the surface Δ_i, which yields the amplitudes of the sine waves in the Fourier spectrum. Specifically, the amplitude of the composite PSD at each wavelength was extracted by taking the square root and dividing by wavelength. Note that a scaling factor of 1.5 was included (Randall, 2004) because a Hanning window was used to produce the PSD. Thus, the function to calculate amplitude from the PSD is

$$\Delta_i = \sqrt{\frac{PSD_i}{1.5\lambda_i}} \tag{5}$$

where i denotes the index in the power-spectrum array. This transformation results in the amplitude spectrum shown in Fig. 3.

In an investigation analyzing the multiscale nature of rough-surface contact using a stacked, or Archard framework, an alternative spectrum was used: the *aspect-ratio spectrum*, which is computed by normalizing the amplitude by wavelength (Jackson, 2010a). The resulting values indicate the aspect ratio of the asperities at each wavelength, thus indicating how pointy or blunt the asperities are at each scale. As shown for elastic and elastic-plastic solutions of wavy surface contact, the pressure required to flatten the asperities is proportional to this ratio, Δ_i/λ_i, to which the variable B has been assigned (Jackson, 2010; Wilson et al., 2010). The aspect-ratio spectrum using this method is shown in Fig. 3b.

If B were constant across all scales, this would indicate that a surface's asperities (the peaks on a rough surface) have the same aspect ratio or shape across all scales. This structure would indicate a self-

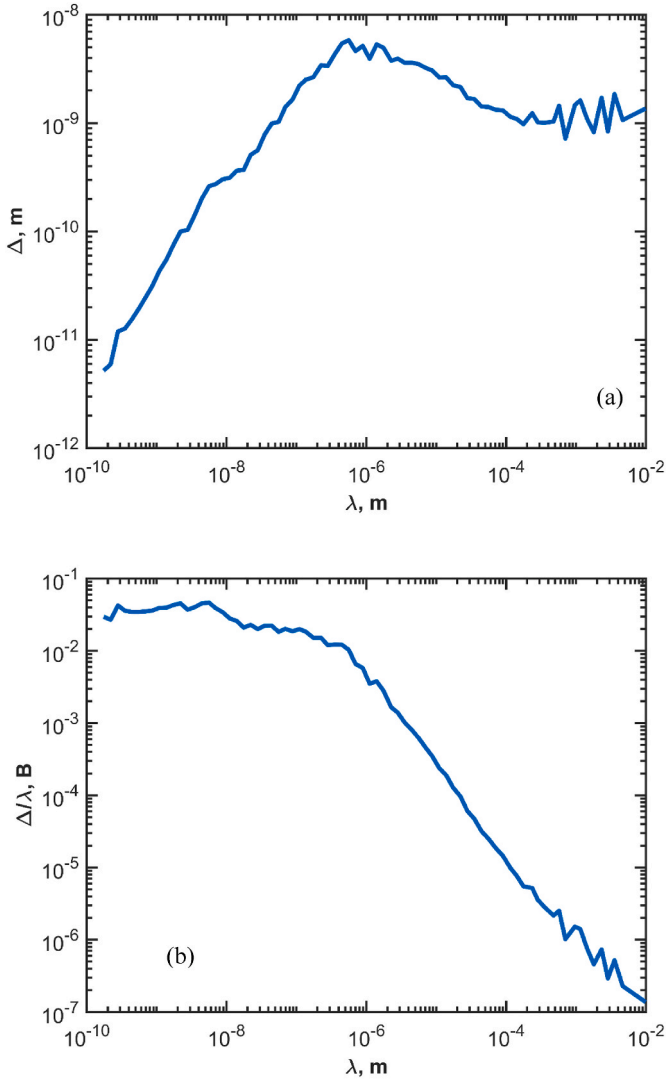

Fig. 3. Amplitude spectrum computed from the composite PSD (a), and the wavelength-normalized spectrum of the surface, also called the aspect-ratio spectrum (b).

similar fractal surface. Alternatively, the plotted B will have a sloped line for self-affine surfaces. In the resulting curve shown in Fig. 3b, the curve is nearly linear over many scales, but bends and becomes horizontal (nearly constant) at smaller wavelengths. Therefore, it appears that the spectrum of the surface is nearly *self-affine* across most size scales, but is nearly *self-similar* at the very smallest wavelengths (below approximately 10 nm).

3. Results and discussion

3.1. Elastic and elastic-plastic models of contact for a real-world multi-scale surface

The amplitude spectrum depicted in Fig. 3 is used as input to the multiscale model as originally described by Archard (1957) and later refined by Ciavarella and Demelio (2001) for fractal elastic contact and by Jackson and Streator (2006) for general elastic-plastic rough surface contact. The latest iteration of the model uses sinusoid-shaped contact models to render the asperities characterized by the waves of the spectrum (Chu et al., 2021; An et al., 2019). The usefulness of this method is that it considers the multiscale nature of surfaces but does not assume that they are purely fractal.

The stacked multiscale models do make several assumptions that result in limitations. The version of the stacked models used in this work assume that all of the asperities at a given scale have uniform amplitudes and wavelengths. Therefore the statistical variation at these scales is not considered. In addition, the model uses an elastic-perfectly plastic wavy contact model that neglects strain hardening. Adhesion is also neglected, but in many cases may not be important. The stacked model assumes that the scales of asperities are stacked in mechanical series, with smaller scale asperities higher in the stack. The scale is defined by the wavelength of the asperities. This would neglect that a small scale wavelength of asperities might actually be taller than other scales and bypass the hierarchal stacking. However the model does capture some important mechanisms, including the coupling and coalescing between adjacent asperities, and that in many cases smaller scale asperities would be superimposed upon larger asperities.

The results of the multiscale model using the full amplitude spectrum are shown in Fig. 4. Although the model predicts different contact areas for different loads, and with and without plastic deformation included, interestingly the contact area appears to converge at the same wavelength of approximately 5.65 nm. This scale or wavelength is also close to the range predicted by Thimons et al. (2021). This wavelength actually corresponds to a peak in the B value shown in the flattened region of Fig. 3b. This wavelength location turns out to also be the maximum value of B (0.0463) for this surface. That this maximum value of B corresponds to the real contact area agrees in concept with a previous simplified version of the model (Jackson, 2010a; Jackson et al., 2009) that theorizes that the real area of contact is approximately equal to force divided by the pressure to flatten the most resistant peaks. In this case the most resistant peaks would be the wavelengths with the highest value of B. Although the scale of the most resistant peaks could shift with scale-dependent strength (See Sect. 3.2). In addition, Fig. 4 shows that the real contact pressures predicted by the elastic-plastic models are approximately eight times higher than the hardness (conventionally three times the yield strength). This is consistent with earlier investigations where contact pressure exceeded the hardness (Krithivasan and Jackson, 2007; Manners, 2008). This occurs from asperities coalescing and resulting in hydrostatic stress rather than deviatoric stress.

In addition to the multi-scale model, four different versions of statistical rough surface contact models were also used to make predictions of the real area of contact (see Table 1). All of the statistical models assume a Gaussian height distribution. The previously described spectral moments and statistical parameters are employed (Eqs. (1)–(4)). The

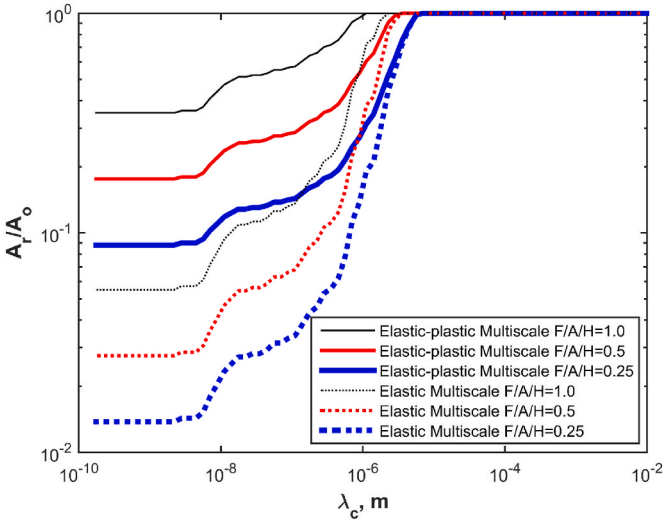

Fig. 4. Real contact area predicted by the stacked multiscale type model as smaller wavelength scales are included.

Table 1
List of considered statistical rough surface contact models.

Asperity Model	Abbreviation	References
Elastic Hertz Statistical Model	Elastic Hertz Stat.	Greenwood and Williamson (1966)
Elastic-plastic Spherical Statistical Model	EP Sphere Stat.	Jackson and Green (2006)
Elastic Sinusoidal Statistical Model	Elastic Sine Stat.	(Chu et al., 2021; Johnson et al., 1985)
Elastic-plastic Sinusoidal Statistical Model	EP Sine. Stat.	(Chu et al., 2021; Ghaednia et al., 2017)

first elastic statistical model employs the elastic Hertz contact solution for the asperities (i.e. the Greenwood and Williamson model, 1966). Elastic-plastic spherical asperity contact was also used in the statistical model for comparison (see (Jackson and Green, 2006) for details). In the elastic-plastic spherical asperity model the ratio between the fully plastic pressure (i.e. hardness) and yield strength decreases as the contact area increases. In addition, some of the taller asperities can be heavily loaded and flattened. In those cases the contact area of a single asperity was limited by the projected area of the spherical asperity (πR^2).

As an alternative, elastic and elastic-plastic sinusoidal asperity models (Johnson et al., 1985) were also used within the statistical framework (details are in (Chu et al., 2021)). There are multiple methods of converting the statistical surface parameters to amplitude, Δ, and wavelength, λ, in the statistical models; the present technique was proven effective in prior work (Chu et al., 2021). In this method the wavelength of the asperities is obtained based on the areal asperity density, or

$$\lambda = \sqrt{\frac{2}{\eta}} \tag{6}$$

Next, the amplitude is predicted based on the asperity curvature as

$$\Delta = \frac{1}{R}\left(\frac{\lambda}{2\pi}\right)^2 \tag{7}$$

Other details of the elastic-plastic sinusoidal asperity model are found in (Chu et al., 2021; Ghaednia et al., 2017).

The statistical model, although probably the most widely used rough surface contact model, is also built upon assumptions and has limitations. The statistical model used in this work assumes that all asperities possess the same average radius of curvature, R, even though they have different heights that are based on a Gaussian distribution. This of course neglects that asperities can vary in curvature, can be elliptical, and not follow the Gaussian distribution. In contrast to statistical models more closely related to the original GW model, the current model does consider some lateral interaction between asperities and substrate deformation by employing elastic and elastic-plastic sinusoidal asperity models as previously noted. One might observe that the stacked and statistical model assumptions differ and complement each other.

The resulting predictions of the elastic and elastic-plastic spherical statistical models are shown in Fig. 5. Note that it is plotted differently than the multiscale model because the statistical models are formulated to predict contact area and force as functions of mean surface separation, whereas the stacked multiscale model makes predictions of contact area directly from the force. As expected, the elastic statistical contact models predict much lower contact areas than the elastic-plastic version of the models. The elastic models appear to be exceptionally dependent on the cut-off wavelength (*i.e.*, λ_c, the smallest considered wavelength of the spectrum). The contact area varies by approximately one order of magnitude when the cutoff wavelength (λ_c) is varied by two orders of magnitude. However, the elastic-plastic models do not appear to vary as much with cutoff wavelength (λ_c). This agrees with the multiscale model findings that at a wavelength on the order of 10 nm the predicted contact

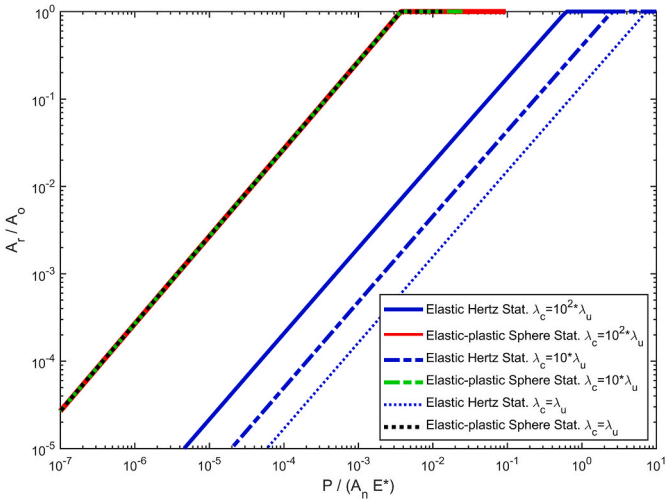

Fig. 5. Real contact area predicted by statistical models as different ranges of wavelength scales are included. The elastic-plastic sphere-based statistical models all fall on nearly the same curve (red, green and black). (For interpretation of the references to colour in this figure legend, the reader is referred to the Web version of this article.)

area levels off, which is approximately 10 times λ_u (the smallest measured wavelength). Following this trend, the prediction of the elastic-plastic statistical model for $100\lambda_u$ appears to start to deviate slightly from the predictions considering smaller scales.

Since the scales of considered spectrum clearly influence the predictions of the multiscale model, a similar evaluation of the statistical models is desirable. Therefore the real contact area from the statistical model was calculated at constant loads as a function of cutoff wavelength. To accomplish this the results for the specific loads must be searched for numerically since, in the statistical model, contact area and force equations are functions of the surface separation, as opposed to the multiscale model which are functions of load. The resulting predictions of the elastic and elastic-plastic spherical and sinusoid asperity statistical model are shown in Fig. 6. From Fig. 6, only the elastic-plastic spherical based statistical models make predictions that are in qualitative agreement with the multiscale models. The slope of the elastic Hertz-based statistical model does start to flatten with smaller scales, but it never becomes horizontal. The elastic sinusoidal-based statistical model is not shown in Fig. 6a, but Fig. 6b shows the isolated results of both the sinusoidal-based statistical models. All versions of the statistical models suggest that with the inclusion of smaller scales of asperities, that the contact area decreases. Both the elastic-plastic spherical and sinusoidal asperity-based statistical models predict a marked increase in contact area compared to the elastic models starting at a cutoff wavelengths (λ_c) below 1–10 μm. The elastic sphere and sinusoidal statistical models do not have a convergence scale or wavelength at which the contact area no longer decreases. This is probably due to the fundamental differences in the statistical and multiscale methodologies, and the spherical and sinusoidal asperity behaviors, which will be discussed in greater detail in Section 3.3. Nonetheless, the elastic-plastic spherical statistical models do predict that the contact area converges or stops decreasing with scale at a cutoff wavelength (λ_c) of approximately 100 nm, which is similar to that predicted by the multiscale models. However, even the contact area predicted by the elastic-plastic spherical-based statistical does decrease in the last decade of included scales. This decrease in contact area at the smallest scales does not appear to decrease lower than when the contact area dipped at approximately 1 μm. As with the multiscale models, the wavelength of convergence of the elastic-plastic sphere-based statistical model appears to be independent of load, at least within the range of loads considered.

The multiscale stacked model and the statistical model are

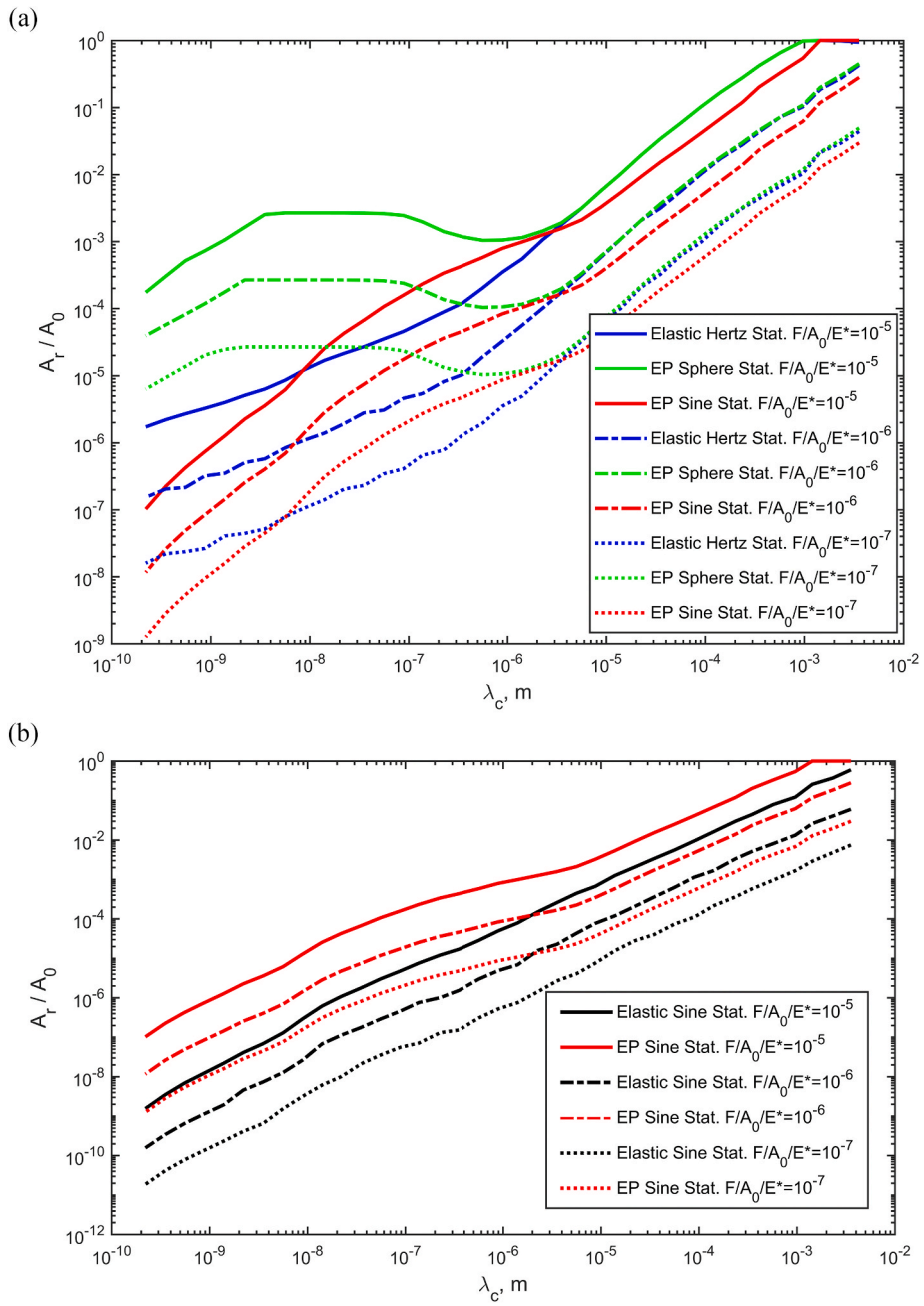

Fig. 6. Real contact area predicted by statistical models for constant loads as a function of the cutoff wavelength based on (a) elastic Hertz, elastic-plastic spherical and elastic-plastic sinusoidal asperities and (b) elastic sinusoidal asperities.

formulated from different mechanical and mathematical frameworks. The multiscale model assumes that the scales of asperities are stacked on each other, but there is no variation in their height within one scale. In contrast, the statistical models assume that all of the asperities are on the same scale (via the radius of curvature) but have different heights following the Gaussian distribution. Despite these differences, they both make similar qualitative predictions about the influence of smaller scales of asperities on contact area. They both predict that the contact area reduces with smaller scales. The stacked multiscale models and elastic plastic spherical statistical model also all predict that a scale of saturation or convergence is reached.

3.2. The effect of including a scale-dependent strength

As mentioned, the strength of many materials often increases at smaller scales. Since rough-surface contact occurs on different scales simultaneously (ranging from the smallest to largest asperities), and at different loads on different scales of asperities, then the asperity contact areas will cover many orders of magnitude in size. In this work the strain-gradient model was used to approximately include the dependence of strength on size scale. This is similar to several previous studies, such as where Jackson (2006) included scale effects in a statistical model, and other similar models that followed using a stacked multiscale framework (Jackson et al., 2015). The present advantage over prior work is the consideration of strain-gradient plasticity over the broad window of surface topography included here. Fleck et al. developed the strain-gradient plasticity theory as a way to consider these scale-dependent effects (Fleck et al., 1994). Using this theory, Nix and Gao (1998) predicted the hardness of a contact to be approximated by:

$$S_y = S_o\sqrt{1+\frac{h^*}{h_p}} \tag{8}$$

where S_o is the macroscopic yield strength, S_y is the corrected scale-dependent yield strength, h^* is a length scale for the effect, and h_p is the depth of plastic deformation caused by the indentation. Eqn 8 is then used as part of the multiscale surface contact model to consider these scale-dependent effects. The main difficulty in using this model is finding the values of h^*. Usually h^* is on the order of micrometers for polycrystalline materials.

First, note that the upper limit of yield strength is often considered to be approximately a tenth of the elastic modulus, E (Ashby et al., 2018). In this case that would be approximately 40–45 GPa, which is in the upper end of what is predicted in the study on the properties of UNCD by Mo et al. (2012) for indentations of a few nanometers. The hardness has been reported to be 88 GPa in another paper which results in strength of approximately 29 GPa at indentations depths of 10–40 nm using a Vickers indenter (Krauss et al., 2001).

For modeling purposes and to approximately demonstrate the influence of scale-dependent strength in this work, a value for h^* of 5 μm is assumed. Then Eq. (8) is used both in the previously described multiscale and statistical models. In the multiscale model, the yield strength is calculated from the deformation of the previous scale using equations relating contact pressure to average surface separation at that scale (Rostami and Jackson, 2013). The value of h_p is then given by:

$$h_p = \Delta - g \tag{9}$$

where from (Rostami and Jackson, 2013)

$$\frac{g}{\Delta} = \left(1-\left(\frac{\bar{p}}{p^*_{ep}}\right)^{A_1\frac{\bar{p}}{p^*_{ep}}+A_2}\right)^{5/2} \tag{10}$$

where

$$A_1 = -0.1\ln\left(\frac{\Delta}{\Delta_c}\right) \tag{11}$$

$$A_2 = \frac{1}{15}\left(\frac{\Delta}{\Delta_c}-1\right)^{0.44} + 0.99^{0.44\left(\frac{\Delta}{\Delta_c}-1\right)} - \frac{1}{2} \tag{12}$$

In the statistical model, h_p is calculated based on the asperity-level interference before the area and force are calculated. Specifically, $h_p = h\text{-}d$.

The resulting contact area predicted by the multiscale model including the strain-gradient strength (Eq. (8)) are shown in Fig. 7 as a function of the cutoff wavelength λ_c (the smallest wavelength included in the model). Note that the nominal pressures in the legend are normalized by the bulk or macro-scale hardness, H, that does not include strain-gradient plasticity. As expected, including the strain-gradient model results in the models predicting lower contact areas, because the effective yield strength is higher. The final contact areas predicted by the strain-gradient elastic-plastic models appear to approach the purely elastic models when all the asperity scales are included, although there are minor differences at intermediate scales. Essentially, for the UNCD surface and properties used in this work, the strain-gradient strength causes the multiscale model to become elastic on the final asperity scales in contact. Also, the contact area appears to converge and not decrease with additional scales at a wavelength between 1 and 10 nm. This suggests that the asperities at scales smaller than this are effectively flattened out. As smaller scales are included the contact area decreases, which also increases the contact pressure. This pressure eventually overcomes all asperities at smaller scales, even despite the increasing hardness at these scales.

Finally, the results of the spherical asperity-based statistical model

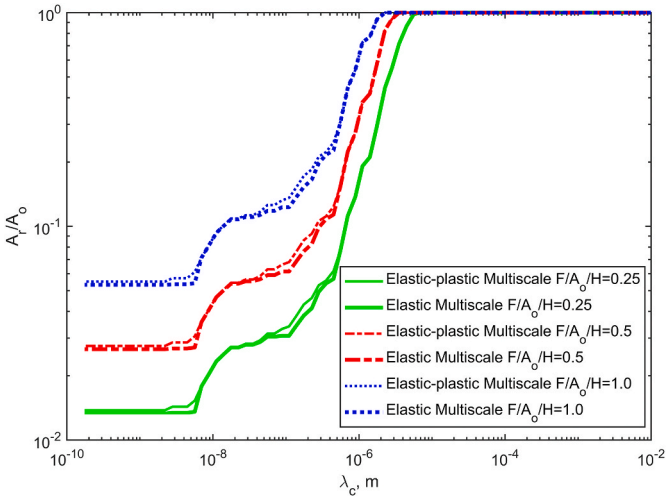

Fig. 7. Scale-dependent real contact area predicted by the stacked multiscale model with a strain-gradient strength. Of course the elastic calculations are unaffected by the strength and so are identical to the curves shown in Fig. 4, but they are shown again here for reference.

including the strain-gradient strength are plotted in Fig. 8 and the sinusoidal asperity-based results are shown in Fig. 9. The statistical models with strain-gradient plasticity were again recalculated at constant loads while varying the cutoff wavelength (λ_c). As with the multiscale models, the contact area predicted when including the scale-dependent strength generally decreases the contact area because the strength is increased. However, in contrast to the multiscale model presented in Fig. 7, the predictions of the elastic-plastic spherical and sinusoidal asperity-based statistical models still differ from the purely elastic models' predictions. The results also suggest that the elastic models depend more on smaller-scale roughness features than when plasticity is included. The smaller spherical asperities get plastically flattened out, even despite their increasing scale-dependent strength. However, at the smallest wavelengths of less than a nanometer, the contact area predicted by the elastic-plastic spherical-based statistical models begin to decrease again. For the elastic-plastic spherical asperity-based statistical model results, the contact area appears to approach a converged prediction at a cutoff wavelength of approximately 0.1 μm, which is earlier than but approximate agreement with the multiscale models, and also in approximate agreement with a previous investigation focused on the effect of roughness scale on adhesion (Thimons et al., 2021). Despite the differences in the underlying assumptions of the multiscale and statistical models, they yield similar trends. Note that this scale of convergence may also depend on the material properties of the surfaces, and the roughness structure outside of these scales.

3.3. Considering all results together

It is interesting to compare the elastic and elastic-plastic curves in Figs. 8 and 9 and the overall results of all versions of the models. All of the models predict an order of magnitude change in contact area with an order of magnitude change in load, which suggests that they predict an approximately linear relationship between contact area and load, as the original statistical and stacked multiscale models did. As the cutoff wavelength (λ_c) decreases, the real contact area begins to generally decrease for all the models; but at different rates that change with the inclusion of smaller scales and in some cases actually increase, but only momentarily. These differences in the statistical model results arise because of the wavy surface asperities used in the statistical models are effectively stiffer than the elastic Hertz and elastic-plastic spherical asperity models. In addition, the elastic-plastic sinusoidal asperity

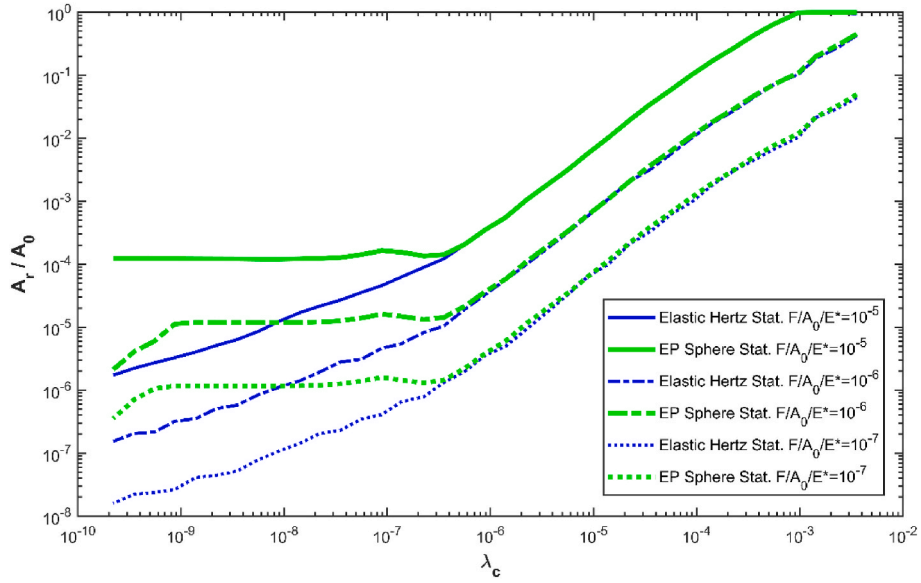

Fig. 8. Scale-dependent real contact area predicted by spherical asperity-based statistical models with the strain-gradient strength included. Once again, elastic calculations are unaffected and are shown here for reference.

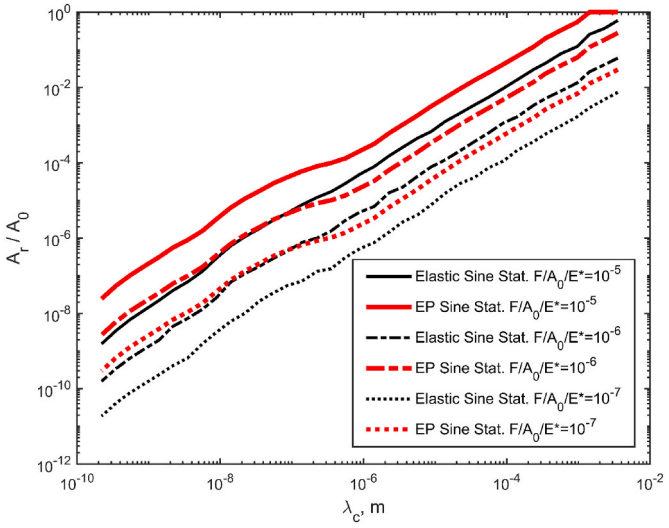

Fig. 9. Real area of contact predicted by strain-gradient sinusoid-based statistical models at constant loads as a function of the cutoff wavelength.

models include the effect of a substrate below them, but the elastic-plastic spherical models do not, which a recent work suggests could be influential (Liu et al., 2023).

The stacked multiscale and spherical asperity based statistical elastic-plastic models predict that, below a certain scale, the roughness no longer influences the real area of contact. In those cases, the contact pressure is sufficient that smaller wavelengths are eventually flattened and do not further affect the contact area. This also holds when scale-dependent strength is considered, but this case comes into closer quantitative agreement with the elastic model, because the strength increases for the smaller asperities. The statistical models are mostly in agreement with the multiscale model trends, except that the elastic Hertz and the sinusoid asperity based statistical models does not converge (level off) as smaller scales of asperities are included.

The results show that most of the statistical models do not converge as cut-off wavelength decreases, except for the elastic-plastic spherical statistical model. This could partly be due to the decoupling of asperities by the statistical model, but even wavy asperities which do include some coupling still do not converge with the inclusion of additional scales. Another possible reason is that the fully plastic pressure (i.e. hardness) decreases with deformation for the sphere contact geometry, where in contrast it increases for sinusoid geometries. The reason for this is that periodic sinusoidal asperities coalesce at higher loads and the stress approaches a hydrostatic state. According to distortion energy yield theory, hydrostatic stress does not cause plastic deformation. This results in the elastic-plastic sinusoid asperities being more resilient than the spherical ones and therefore less likely to flatten with the inclusion of smaller scales.

Most importantly, the statistical model uses a different mathematical framework that does not consider how smaller-scale asperities might be under higher loads, as the multiscale model does. In reality, smaller asperities or roughness features are usually superimposed upon larger features. This is similar to the concept of self-similarity in fractal roughness. In the multiscale model the pressure increases with the stacking of each smaller scale of asperities and results in a higher likelihood of being flattened. Since the statistical models do not consider this, their results should be given less weight in determining the trends that apply to real-world surfaces. More complex statistical models that include variation of curvature might correct this (Bush et al., 1975).

Other than the cases of sinusoidal and elastic spherical statistical models, the predictions suggest that most materials will have a certain scale of features below which the roughness will no longer reduce the area of contact. Of course this may vary depending on the particular geometrical structure of the surfaces and the material properties. As suggested in Ref. (Jackson, 2010), this might depend on the overall slope of the surface spectrum, which relates to the self-affinity or self-similarity of the spectrum. In general, if surfaces are more self-affine and fractal-like in nature, than the asperities will have taller and thinner aspect ratios with smaller scales, and thus be more resistant to flattening. For the nearly complete surface spectrum considered in this work, the surface appeared self-affine at large scales, but then become more self-similar at smaller scales (see Fig. 3 where the asperity aspect ratio B approaches a constant value at small wavelengths). This enables the ability of the increasing contact pressure to overcome the smaller asperities and flatten them. Note that real surfaces are not exactly fractal and the behavior may deviate from that predicted by pure fractal-based modeling. Adhesion is also neglected in this work, though depending on the surface energies, could be important in some cases. Despite not including adhesion, the predictions of a critical scale of roughness are

consistent with what has been observed experimentally in an adhesive contact (Thimons et al., 2021).

4. Conclusions

In this investigation, multiscale stacked and statistical models of rough-surface contact were implemented by using the nearly complete spectrum of a rough surface. As expected, all the models predict that contact area will decrease as smaller scales of asperities are included. The elastic Hertz asperity-based and sinusoidal asperity-based statistical models predicted that contact area continues to decrease as smaller and smaller scales; however, all other models (elastic-plastic spherical asperity-based statistical, elastic multiscale, elastic-plastic multiscale) predicted that the contact area flattened out, or converged, at a particular wavelength. Even when scale-dependent strength is considered, this convergence still occurred, though there was a shift in the relevant size scale. It is probable that the critical size at which convergence occurs will vary based on the particular geometrical and material structure of a surface. The physical implication of this result is that, in some cases, roughness need only be considered down to a certain critical size, below which it will have no effect on contact area. Since the statistical models do not consider the scaled hierarchal nature of surfaces, they may be less able to make this prediction accurately. Additionally, all of the models predict that, while plasticity does allow the contact area to converge and reduce the pressure in comparison to the elastic case, the hardness does not limit the contact pressure.

Declaration of competing interest

The authors declare that they have no known competing financial interests or personal relationships that could have appeared to influence the work reported in this paper.

Data availability

Data will be made available on request.

Acknowledgements

T. D. B. Jacobs acknowledges support from the National Institute for Occupational Safety and Health (NIOSH) under award R21 OH012126.

References

An, B., Wang, X., Xu, Y., Jackson, R.L., 2019. Deterministic elastic-plastic modelling of rough surface contact including spectral interpolation and comparison to theoretical models. Tribol. Int. 135, 246–258. https://doi.org/10.1016/j.triboint.2019.02.039.
Archard, J., 1957. Elastic deformation and the laws of friction. Proc. Roy. Soc. Lond. Math. Phys. Sci. 243, 190–205.
Ashby, M.F., Shercliff, H., Cebon, D., 2018. Materials: Engineering, Science, Processing and Design. Butterworth-Heinemann.
Bhushan, B., Majumdar, A., 1992. Elastic-plastic contact model for bifractal surfaces. Wear 153, 53–64.
Borodich, F.M., Pepelyshev, A., Savencu, O., 2016. *Statistical approaches to description of rough engineering surfaces at nano and microscales*. Tribology International 103, 197–207.
Borri, C., Paggi, M., 2015. Topological characterization of antireflective and hydrophobic rough surfaces: are random process theory and fractal modeling applicable? J. Phys. Appl. Phys. 48, 045301.
Bowden, F.P., Tabor, D., 1939. The area of contact between stationary and moving surfaces. Proc. Roy. Soc. Lond. Math. Phys. Sci. 169, 391–413.
Broitman, E., 2016. Indentation hardness measurements at macro-, micro-, and nanoscale: a critical overview. Tribol. Lett. 65, 23. https://doi.org/10.1007/s11249-016-0805-5.
Bush, A.W., Gibson, R.D., Thomas, T.R., 1975. The elastic contact of a rough surface. Wear 35, 87–111. https://doi.org/10.1016/0043-1648(75)90145-3.
Christopher, A.B., et al., 2018. Multiscale analyses and characterizations of surface topographies. CIRP Annals 67, 839–862. https://doi.org/10.1016/j.cirp.2018.06.001.
Chu, N.R., Jackson, R.L., Wang, X., Gangopadhyay, A., Ghaednia, H., 2021. Evaluating elastic-plastic wavy and spherical asperity-based statistical and multi-scale rough surface contact models with deterministic results. Materials 14, 3864.
Ciavarella, M., Demelio, G., 2001. Elastic multiscale contact of rough surfaces: archard's model revisited and comparisons with modern fractal models. J. Appl. Mech. 68, 496–498.
Dalvi, S., et al., 2019. Linking energy loss in soft adhesion to surface roughness. Proc. Natl. Acad. Sci. USA 116, 25484–25490.
Fleck, N.A., Muller, G.M., Ashby, M.F., Hutchinson, J.W., 1994. Strain gradient plasticity: theory and experiment. Acta Metall. Mater. 42, 475–487.
Ghaednia, H., et al., 2017. A review of elastic–plastic contact mechanics. Appl. Mech. Rev. 69 https://doi.org/10.1115/1.4038187.
Green, I., 2019. Exact spectral moments and differentiability of the weierstrass-mandelbrot fractal function. J. Tribol. 142 https://doi.org/10.1115/1.4045452.
Greenwood, J.A., Williamson, J.P., 1966. Contact of nominally flat surfaces. Proc. Roy. Soc. Lond. Math. Phys. Sci. 295, 300–319.
Gujrati, A., Khanal, S.R., Pastewka, L., Jacobs, T.D.B., 2018. Combining TEM, AFM, and profilometry for quantitative topography characterization across all scales. ACS Appl. Mater. Interfaces 10, 29169–29178. https://doi.org/10.1021/acsami.8b09899.
Gujrati, A., Khanal, S.R., Pastewka, L., Jacobs, T.D.B., 2022. Ultrananocrystalline Diamond (UNCD) (Version 2). https://doi.org/10.57703/ce-5cz7a. https://contact.engineering.
Jackson, R.L., 2006. The effect of scale-dependent hardness on elasto-plastic asperity contact between rough surfaces. Tribol. Trans. 49, 135–150. https://doi.org/10.1080/05698190500544254.
Jackson, R.L., 2010. An analytical solution to an archard-type fractal rough surface contact model. Tribol. Trans. 53, 543–553. https://doi.org/10.1080/10402000903502261.
Jackson, R.L., Green, I., 2006. A statistical model of elasto-plastic asperity contact between rough surfaces. Tribol. Int. 39, 906–914. https://doi.org/10.1016/j.triboint.2005.09.001.
Jackson, R.L., Streator, J.L., 2006. A multi-scale model for contact between rough surfaces. Wear 261, 1337–1347.
Jackson, R.L., Malucci, R.D., Angadi, S., Polchow, J.R., 2009. Proceedings of the 55th IEEE Holm Conference on Electrical Contacts. IEEE, pp. 28–35.
Jackson, R.L., Crandall, E.R., Bozack, M.J., 2015. Rough surface electrical contact resistance considering scale dependent properties and quantum effects. J. Appl. Phys. 117, 195101.
Jacobs, T., Junge, T., Pastewka, L., 2017. Quantitative characterization of surface topography using spectral analysis. Surf. Topography: Metrol. Prop. 5, 013001.
Johnson, K., Greenwood, J., Higginson, J., 1985. The contact of elastic regular wavy surfaces. Int. J. Mech. Sci. 27, 383–396.
Kalin, M., Pogačnik, A., Etsion, I., Raeymaekers, B., 2016. Comparing surface topography parameters of rough surfaces obtained with spectral moments and deterministic methods. Tribol. Int. 93, 137–141.
Kogut, L., Jackson, R.L., 2005. A comparison of contact modeling utilizing statistical and fractal approaches. J. Tribol. 128, 213–217. https://doi.org/10.1115/1.2114949.
Krauss, A.R., et al., 2001. Ultrananocrystalline diamond thin films for MEMS and moving mechanical assembly devices. Diam. Relat. Mater. 10, 1952–1961. https://doi.org/10.1016/S0925-9635(01)00385-5.
Krithivasan, V., Jackson, R.L., 2007. An analysis of three-dimensional elasto-plastic sinusoidal contact. Tribol. Lett. 27, 31–43.
Liu, S., Dorcy, N., Wang, Q., Chung, Y.-W., Berkebile, S., 2023. Contacting micro asperity of a deformable surface. J. Tribol. 1–31. https://doi.org/10.1115/1.4062576.
Majumdar, A., Bhushan, B., 1991. Fractal Model of Elastic-Plastic Contact between Rough Surfaces. J. Tribol. 113, 1–11. https://doi.org/10.1115/1.2920588.
Majumdar, A., Tien, C.L., 1990. Fractal characterization and simulation of rough surfaces. Wear 136, 313–327. https://doi.org/10.1016/0043-1648(90)90154-3.
Mandelbrot, B., 1967. How long is the coast of Britain? Statistical self-similarity and fractional dimension. Science 156, 636–638.
Manners, W., 2008. Plastic deformation of a sinusoidal surface. Wear 264, 60–68.
McCool, J., 1982. Finite difference spectral moment estimation for profiles the effect of sample spacing and quantization error. Precis. Eng. 4, 181–184.
McCool, J.I., 1986. Comparison of models for the contact of rough surfaces. Wear 107, 37–60. https://doi.org/10.1016/0043-1648(86)90045-1.
McCool, J.I., 1987. Relating Profile Instrument Measurements to the Functional Performance of Rough Surfaces. J. Tribol. 109, 264–270. https://doi.org/10.1115/1.3261349.
Mo, Y., Stone, D., Szlufarska, I., 2012. Strength of ultrananocrystalline diamond controlled by friction of buried interfaces. J. Phys. Appl. Phys. 45, 069501 https://doi.org/10.1088/0022-3727/45/6/069501.
Mohr, M., et al., 2014. Young's modulus, fracture strength, and Poisson's ratio of nanocrystalline diamond films. J. Appl. Phys. 116, 124308 https://doi.org/10.1063/1.4896729.
Müser, M.H., Nicola, L., 2022. Modeling the surface topography dependence of friction, adhesion, and contact compliance. MRS Bull. 47, 1221–1228. https://doi.org/10.1557/s43577-022-00468-2.
Müser, M.H., et al., 2017. Meeting the contact-mechanics challenge. Tribol. Lett. 65, 1–18.
Nix, W.D., Gao, H., 1998. Indentation size effects in crystalline materials: a law for strain gradient plasticity. J. Mech. Phys. Solid. 46, 411–425.
Papangelo, A., Ciavarella, M., 2021. A criterion for the effective work of adhesion in loading and unloading of adhesive soft solids from rough surfaces. Tribol. Lett. 69, 9. https://doi.org/10.1007/s11249-020-01390-x.
Patil, D.B., Eriten, M., 2014. Effects of interfacial strength and roughness on the static friction coefficient. J. T. l. 56, 355–374.
Persson, B.N., 2006. Contact mechanics for randomly rough surfaces. Surf. Sci. Rep. 61, 201–227.

Persson, B., Tosatti, E., 2001. The effect of surface roughness on the adhesion of elastic solids. J. Chem. Phys. 115, 5597–5610.
Randall, R.B., 2004. State of the art in monitoring rotating machinery-part 1. Sound Vib. 38, 14–21.
Richardson, L.F., 1961. The problem of contiguity: an appendix to statistics of deadly quarrels. Gen. Syst. Yearbk. 6, 139–187.
Rostami, A., Jackson, R.L., 2013. Predictions of the average surface separation and stiffness between contacting elastic and elastic–plastic sinusoidal surfaces. Proc. IME J. J. Eng. Tribol. 227, 1376–1385. https://doi.org/10.1177/1350650113495188.
Röttger, M.C., et al., 2022. Contact.engineering—create, analyze and publish digital surface twins from topography measurements across many scales. Surf. Topogr. Metrol. Prop. 10, 035032 https://doi.org/10.1088/2051-672X/ac860a.
Sanner, A., Nöhring, W.G., Thimons, L.A., Jacobs, T.D.B., Pastewka, L., 2022. Scale-dependent roughness parameters for topography analysis. Applied Surface Science Advances 7, 100190. https://doi.org/10.1016/j.apsadv.2021.100190.
Sayles, R.S., Thomas, T.R., 1978. Surface topography as a nonstationary random process. Nature 271, 431–434. https://doi.org/10.1038/271431a0.
Thimons, L.A., Gujrati, A., Sanner, A., Pastewka, L., Jacobs, T.D.B., 2021. Hard-material adhesion: which scales of roughness matter? Exp. Mech. 61, 1109–1120. https://doi.org/10.1007/s11340-021-00733-6.
Venugopalan, S., Nicola, L., 2019. Indentation of a plastically deforming metal crystal with a self-affine rigid surface: a dislocation dynamics study. Acta Mater. 165, 709–721.
Venugopalan, S.P., Irani, N., Nicola, L., 2019. Plastic contact of self-affine surfaces: persson's theory versus discrete dislocation plasticity. J. Mech. Phys. Solid. 132, 103676 https://doi.org/10.1016/j.jmps.2019.07.019.
Violano, G., Afferrante, L., Papangelo, A., Ciavarella, M., 2021. On stickiness of multiscale randomly rough surfaces. J. Adhes. 97, 509–527. https://doi.org/10.1080/00218464.2019.1685384.
Whitehouse, D., 2001. Fractal or fiction. Wear 249, 345–353.
Wilson, W.E., Angadi, S.V., Jackson, R.L., 2010. Surface separation and contact resistance considering sinusoidal elastic-plastic multi-scale rough surface contact. Wear 268, 190–201.
Xu, Y., Chen, Y., Zhang, A., Jackson, R.L., Prorok, B.C., 2018. A new method for the measurement of real area of contact by the adhesive transfer of thin Au film. Tribol. Lett. 66, 1–20.
Xu, Y., Jackson, R.L., Chen, Y., Zhang, A., Prorok, B.C., 2020. A comparison of nanoscale measurements with the theoretical models of real and nominal contact areas. Proc. IME J. J. Eng. Tribol. 234, 1735–1745.
Zhang, X., Jackson, R.L., 2017. *An Analysis of the Multiscale Structure of Surfaces with Various Finishes*. Tribology Transactions 60 (1), 121–134.
Zhang, W., Lu, Z., Chen, Y., Zhang, Y., 2022. Contact analysis between rough surfaces considering the size-affected deformation behaviour of multi-scale asperities. Tribol. Int. 172, 107592.